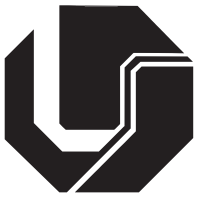

UNIVERSIDADE FEDERAL DE UBERLÂNDIA
FACULDADE DE ENGENHARIA MECÂNICA
GRADUAÇÃO EM ENGENHARIA MECÂNICA

Active crack control approach applied to a horizontal rotating machine

Iago Alves Pereira

Uberlândia

2022

Iago Alves Pereira

Técnica de controle atívo para controle de trinca aplicado em uma máquina rotativa horizontal

Projeto de fim de curso apresentado ao Programa de graduação em Engenharia Mecânica da Universidade Federal de Uberlândia, como parte dos requisitos para obtenção do grau de Bacharel em Engenharia Mecânica.

Área de Concentração: Vibrações e Projeto Mecânico
Linha de pesquisa: Dinâmica de Máquinas Rotativas

Prof. Dr. Aldemir Aparecido Cavalini Jr,
Orientador

Prof. Dr. Núbia dos Santos Saad
Coordenador do PG em Engenharia Mecânica

Uberlândia
2022

Iago Alves Pereira

Técnica de controle atívo para controle de trinca aplicado em uma máquina rotativa horizontal

Projeto de fim de curso apresentado ao Programa de Graduação em Engenharia Mecânica da Universidade Federal de Uberlândia, como parte dos requisitos para obtenção do grau de Bacharel em Engenharia Mecânica.

Área de Concentração: Vibrações e Projeto Mecânico
Linha de pesquisa: Dinâmica de Máquinas Rotativas

Uberlândia, 04 de março de 2022.

Banca examinadora:

Prof. Dr. Aldemir Aparecido Cavalini Jr., Orientador (UFU)
Ms. Jefferson Silva Barbosa
Prof. Dr. Leandro de Souza Leão, Co-orientador (UFSJ)
Dr. Vergílio Torezan Silingardi Del Claro

Acknowledgements

I respectfully ask for the readers to excuse me because I will write this section in Portuguese to properly translate my gratitude to all Brazilians that have helped me during this long and challenging journey.

Primeiramente, gostaria de agradecer aos meus pais Angélica e Renato por me proporcionar toda estrutura possível (e às vezes impossível) para que eu pudesse focar em meus estudos e tentar fazer o meu melhor sempre. Graças às condições que vocês me deram, eu tive a oportunidade de ingressar em uma universidade federal e finalizar meu bacharel com desempenho acima da média.

Também gostaria de agradecer a minha eterna companheira Isabela que sempre me apoiou e me consolou nos momentos difíceis dessa jornada. Foram muitos fins de semana e feriados que passamos distantes devido às minhas exigências para com este curso de Engenharia. Apesar da minha ausência, você sempre foi muito compreensiva e companheira.

Agradeço aos bons professores que compõem o quadro de profissionais da FEMEC e que dedicam-se diariamente para entregar o melhor que podem para os estudantes. Em especial, agradeço à Prof. Núbia que faz um trabalho espetacular na coordenação e não mede esforços para ajudar os estudantes com qualquer que sejam as nossas demandas.

Agradeço aos meus colegas de graduação que me ajudaram durante o curso de Engenharia Mecânica, especialmente ao meu grande amigo Arturo. Muito obrigado pela parceria e companheirismo de sempre. Sem vocês esse curso teria sido muito mais difícil!

Agradeço também a minha grande amiga Lara David que me orientou em todo o processo de inscrição para alguns programas de doutorado nos Estados Unidos. Foram meses de preparação, adequação e correção de uma série de documentos

para aplicação. No fim, nossos esforços me asseguraram uma bolsa de doutorado no 11° melhor programa de pós-graduação em Eng. Mecânica do mundo. Sem sombra de dúvidas, todo esse processo sem você teria sido muito mais desafiador sem a sua ajuda!

Gostaria de agradecer ao Prof. Aldemir por me proporcionar a oportunidade de fazer parte do LMEst, local onde iniciei minha jornada como estudante e me formei engenheiro. Agradeço também ao Prof. Valder por sempre ser muito aberto e receptivo e por me ajudar todas as vezes que pedi. Sem sombra de dúvidas, o senhor me inspira.

Agradeço aos meus amigos e irmãos Vergílio e Sorriso. Com vocês eu me diverti e aprendi muito! Muito obrigado pelas horas de dedicação e por acreditarem em mim desde o início. Sem sombra de dúvidas, vocês foram as pessoas que mais contribuíram para minha formação profissional. Vocês foram meus verdadeiros professores.

Agradeço também ao meu "velho" companheiro Felipe. Você foi primordial para que eu e o Sorriso conseguíssemos realizar este trabalho. Muito obrigado por nos orientar, acompanhar os experimentos e tirar minhas dúvidas sobre Controle sempre que possível.

Agradeço também ao André e ao Batuta. Presenciar o profissionalismo diário de vocês durante meu tempo no LMEst sempre me inspirou e motivou a ser melhor. Vocês são umas das minhas principais referências em excelência e seriedade.

Agradeço aos meus companheiros do LMEst que sempre foram muito abertos e receptivos comigo. Todos vocês contribuíram com a minha formação durante esses anos.

Por fim mas não menos importante, gostaria de agradecer ao Prof. Pedro Assis que foi muito solícito e gentil comigo todas as vezes que precisei de orientações na parte de Controle de Sistemas Dinâmicos. Na reta final do curso, as orientações do Prof. Pedro foram essenciais para que eu conseguisse garantir minha bolsa de estudos para fazer doutorado na Universidade de Michigan. Prof. Pedro, serei eternamente grato por sua assistência. Essa oportunidade que conseguimos alcançar mudará minha vida! Professores como você me inspiram a trabalhar ainda mais. Obrigado por fazer parte da nossa FEMEC!

Muito obrigado a todos vocês!

”I know very well that I am standing on shoulder of giants.”

By Michael Bublé before singing Sinatra and Bart Howard’s "Fly Me to the Moon"

Abstract

Pereira, I. A. *Active crack control approach applied to a horizontal rotating machine*. Bachelor's Thesis - Federal University of Uberlândia, March 2022.

The present contribution proposes a active vibration control technique devoted to shafts with cracks aiming to minimize their propagation. The existence of a crack in rotating shafts can be characterized by $2X$ and $3X$ super-harmonic amplitudes in the vibration responses of the rotor, which can increase as the crack propagates along the shaft's cross-section. A proportional-integral-derivative (PID) control technique is applied to suppress the $2X$ and $3X$ vibration amplitudes of a cracked shaft, which is performed by using a band-pass filter applied to the vibration displacement responses measured in the rotor. Numerical and experimental results are obtained through a representative finite element (FE) model of a horizontal rotor. In this case, electromagnetic actuators (EMA) are used to apply the control effort on the rotor. The Mayes model is applied for simulating the breathing behavior of the transverse crack. The linear fracture mechanics theory is considered to correlate the crack depth with the corresponding additional rotor flexibility. Both numerical and experimental results demonstrate the possibility of reducing the effects of a transverse crack through active control on the dynamic behavior of a rotating machine. Moreover, it is shown that the proposed control law is capable of controlling the crack effects with the rotor operating in different rotation speeds.

Keywords: Rotating machines. Transverse cracks. Vibration Control. PID controller. Electromagnetic Actuators.

Resumo

Pereira, I. A. *Técnica de controle atívo para controle de trinca aplicado em uma máquina rotativa horizontal*. Projeto de Fim de Curso - Universidade Federal de Uberlândia, Março 2022.

A presente contribuição propõe uma técnica de controle ativo de vibração para eixos com trincas visando minimizar sua propagação. A existência de uma trinca em eixos rotativos pode ser caracterizada pela presença de super-harmônicos $2X$ e $3X$ nas respostas de vibração do rotor, que podem aumentar à medida que a trinca se propaga ao longo da seção transversal do eixo. Uma técnica de controle proporcional-integral-derivativo (PID) é aplicada para suprimir as amplitudes de vibração de $2X$ e $3X$ de um eixo trincado, o que é realizado usando um filtro passa-banda aplicado às respostas de vibração medidas no rotor. Resultados numéricos e experimentais são obtidos através de um modelo representativo de elementos finitos (FE) de um rotor horizontal. Neste caso, atuadores eletromagnéticos (EMA) são utilizados para aplicar o esforço de controle no rotor. O modelo de Mayes é aplicado para simular o comportamento *breathing* da trinca transversal. A teoria da mecânica da fratura linear é considerada para correlacionar a profundidade da trinca com a correspondente flexibilidade adicional do rotor. Tanto os resultados numéricos quanto os experimentais demonstram a possibilidade de reduzir os efeitos de uma trinca transversal através do controle ativo no comportamento dinâmico de uma máquina rotativa. Além disso, mostra-se que a lei de controle proposta é capaz de controlar os efeitos da trinca com o rotor operando em diferentes velocidades de rotação.

Palavras-chave: Máquinas Rotativas. Trinca Transversal. Controle de Vibração Ativo. Controlador PID. Atuadores Eletromagnéticos.

Publications

The research done on this Bachelor's Thesis directly resulted on, or aided in developing, the publications listed below:

Journal Papers

- L. S. Leão., **I. A. Pereira**, F. C. Carvalho, A. A. Cavalini Jr. and V. Steffen Jr., "Active crack control approach applied to a horizontal rotating machine", Journal of Vibration and Control, (2022) - PAPER ACCEPTED

Conference Presentation and Annals

- **I. A. Pereira**, L. S. Leão, L. C. Sicchieri, V. N. Carvalho, A. A. Cavalini Jr. and V. Steffen Jr., "DYNAMIC CHARACTERIZATIONS OF ELECTROMAGNETIC ACTUATORS", Proceedings of COBEM 2019 – 25th ABCM International Congress on Mechanical Engineering, Uberlândia, Brazil, 20th – 25th October 2019.
  DOI: 10.26678/ABCM.COBEM2019.COB2019-1691

- L. S. Leão., **I. A. Pereira**, A. A. Cavalini Jr. and V. Steffen Jr., "A MODEL-BASED CRACK IDENTIFICATION APPROACH", Proceedings of COBEM 2019 – 25th ABCM International Congress on Mechanical Engineering, Uberlândia, Brazil, 20th – 25th October 2019.
  DOI: 10.26678/ABCM.COBEM2019.COB2019-0814

- **I. A. Pereira**, L. S. Leão, F. C. Carvalho, A. A. Cavalini Jr. and V. Steffen Jr., "VIBRATION SUPPRESSION ON A ROTATING MACHINE BY THE USE OF ELECTROMAGNETIC ACTUATORS AND A PID CONTROLLER", Proceedings of CREEM 2019 – 26th Congresso Nacional de Estudantes de Engenharia Mecânica, Ilhéus, Brazil, 19th – 23th August 2019.
  DOI: 10.26678/ABCM.CREEM2019.CRE2019-0073

- **I. A. Pereira**, L. S. Leão, A. A. Cavalini Jr. and V. Steffen Jr., "COMPARAÇÃO DE AMPLIFICADORES DE CORRENTE PARA SISTEMAS DE CONTROLE ATIVO DE VIBRAÇÃO", Proceedings of CREEM 2019 – 26th Congresso Nacional de

Estudantes de Engenharia Mecânica, Ilhéus, Brazil, 19th – 23th August 2019.
DOI: 10.26678/ABCM.CREEM2019.CRE2019-0075

Other contributions produced during my undergraduate studies but not directly linked to this Bachelor's Thesis are listed below:

Patents

- **I. A. Pereira**, V. T. S. Del Claro, T. T. S. Del Claro, A. A. Cavalini Jr. and V. Steffen Jr., "ESTRUTURA MODULAR DE FIXAÇÃO DE ATUADORES ELETROMAGNÉTICOS RADIAIS PARA ENSAIOS NÃO-DESTRUTIVOS E SIMULAÇÕES DE FALHAS EM MÁQUINAS ROTATIVAS SEM DESMONTAGEM DE MANCAIS", Current Assignee: Petroleo Brasileiro SA Petrobas - BR 10 2021 022899 7

Conference Presentation and Annals

- **I. A. Pereira**, V. T. S. Del Claro, L. S. Leão, F. V. de Oliveira, A. A. Cavalini Jr. and V. Steffen Jr., "A DIDACTIC TEST-RIG FOR TEACHING VIBRATION MODES", Proceedings of COBEM 2019 – 25th ABCM International Congress on Mechanical Engineering, Uberlândia, Brazil, 20th – 25th October 2019.
DOI: 10.26678/ABCM.COBEM2019.COB2019-1668

Table of Contents

List of Figures

List of Tables

List of Symbols

Rotor Model

ΔK	Stiffness matrix associated with the crack
Ω	Rotating speed
D	Damping matrix
D_g	Gyroscopic effect
F_u	Unbalance force
$F_{control}$	Control Forces
K	stiffness matrix
M	Mass matrix
q	Generalized coordinate vector
W	Weight force

Electromagnetic Force and Controller

δ	Shaft vibration
μ_o	Vacuum magnetic permeability
μ_r	Relative magnetic permeability
a, b, c, d, e,f	Dimensions of the actuator
F_{ema}	Electromagnetic force
I	Electrical current
K_D	Derivative gain
K_I	Integral gain
K_p	Proportional gain
N	Number of windings

Optimization Parameters

ξ_1, ξ_2, ξ_3,ξ_4	Modal damping factors associated with the first four vibration modes
F_{DE}	Objective function used in the minimization process

$FRF_{exp,k}$	Experimental FRFs
$FRF_{num,k}$	Numerical FRFs
$k_{t_{coup}}$	Torsional stiffness due to the coupling between the shaft and the electric motor.
$k_{XX_{B1}}$,$k_{XX_{B2}}$	Stiffness along horizontal direction of each bearing
$k_{ZZ_{B1}}$,$k_{ZZ_{B2}}$	Stiffness along vertical direction of each bearing

Transverse Crack Model

$k_{\eta_{Mayes}}$	Angular dependent stiffness along the η direction
ΔK	Stiffness matrix associated with the crack
$\mathbf{k}_{F_{Mayes}}$	Stiffness of the shaft with crack in fixed coordinates
$\mathbf{k}_{R_{Mayes}}$	Stiffness of the shaft with crack in rotating coordinates
ω_d	Damped natural frequency
ω_n	Undamped natural frequency
Ω	System rotation speed
k_η	Stiffness of the shaft with a crack along the η direction
K_c	Stiffness matrix of the shaft element with crack
k_o	Stiffness of the healthy shaft
K_p	Stiffness matrix of the pristine shaft element
$k_{\xi_{Mayes}}$	Stiffness of the shaft with a crack along the ξ direction
$k_{FMayes11}$	Stiffness terms included in the FE formulation to obtain the stiffness matrix K_c
$k_{FMayes12}$	Stiffness terms included in the FE formulation to obtain the stiffness matrix K_c

Chapter 1

Introduction

Turbomachines describe devices that transfer energy between a rotor and a fluid, including compressors, steam, gas, hydraulic, and wind turbines, Logan Jr (1993). According to Demierre et al. (2012), Demierre et al. (2014), and Fitzgerald et al. (2018), the efficiency of these rotating machines have been improved along the last years. Even though, commonly rotor fault conditions such as unbalance, misalignment, rubbing, and the so-called transversal cracks, continue to affect the performance of these rotating machines, Boyko et al. (2010). Thus, considerable academic efforts were dedicated to understanding the dynamic behavior of faulty rotating shafts and to develop fault detection techniques, Greco et al. (1978), Kottke, Menning (1981), Klompas (1983), Dimarogonas (1996), Ostachowicz, Krawczuk (2001), Carden, Fanning (2004), Jeon et al. (2019), and CavaliniJr et al. (2020).

According to Dimarogonas et al. (2013), the existence of transverse cracks in rotating shafts leads to mechanical stiffness becoming variable. In this case, the mechanical stiffness of the shaft changes according to its angular position. Mathematical models have been presented in the literature to simulate the dynamic behavior of shafts with transversal cracks, such as the Mayes model and FLEX models associated with the FE formulation to representing rotating machines, Grabowski (1984) and Bachschmid et al. (2000). Consequently, damage detection methodologies based on mathematical models were developed and tested over the years.

Concerning crack detection techniques, Bachschmid et al. (2000) were able to predict the depth and location of a transverse crack based on the $1X$, $2X$, and $3X$ superharmonic vibration responses of a horizontal rotating machine. The proposed crack

identification method was based on the least-squares approach and the mathematical model of the rotor. The technique was able to predict satisfactorily both the depth and location of a transverse crack even when using the vibration responses measured on the bearings, which is more realistic in the context of industrial applications.

Friswell et al. (2010) proposed an efficient crack detection technique based on recurrence plots devoted to rotating machines. The considered test rig used active magnetic bearings (AMBs) to levitate the rotating shaft with a transverse crack. The AMBs were also used for applying sinusoidal forces with frequencies able to induce vibration responses containing combinations of both excitation frequencies and angular velocity of the rotor.

Nicoletti et al. (2018) detected incipient cracks in rotors by combining the combination resonances approach with the Approximated Entropy algorithm. According to the authors, ApEn is able to quantify patterns and correspondences between samples of the same time series to detect anomalies. The combination resonances approach is used to highlight the dynamic behavior of the crack on the shaft vibration responses. Therefore, the ApEn algorithm can be used to detect the presence of such resonances. The proposed approach was numerically and experimentally evaluated, demonstrating the efficiency of the conveyed methodology.

Leão et al. (2019) studied a crack detection approach based on a modal state observer. The most affected vibration modes due to the faulty condition of the rotor were determined by applying a kernel density estimator in the modal vibration responses that had been estimated by using the modal state observer. Satisfactory results were obtained using the proposed crack detection approach.

Control techniques have also been applied to rotating machines over the years for vibration mitigation purposes, as presented by Karakaya, Karakas (2014), Pesch et al. (2014), Jung, DeSmidt (2018), Camino, Santos (2019), and Carvalho et al. (2021). In general, vibration control of rotating machines can be performed based on passive, semi-active, and active strategies.According to Cavalini et al. (2011), passive techniques usually employ absorbers or isolators for vibration attenuation purposes. Despite their low cost and easy application, these devices can cover only a limited frequency bandwidth of the system response, being unable to adapt their characteristics to any change in the system. Otherwise, semi-active techniques aim at changing the

physical parameters of rotating machines, Jung, DeSmidt (2018). Finally, active control strategies are based on the application of dynamic forces to the rotating shaft to reduce its lateral vibrations, Tammi (2007).

Ribeiro et al. (2015) applied a viscoelastic material on the bearings of a rotating machine for passive vibration attenuation purposes. The vibration responses and transmissibility were obtained considering ball and hydrodynamic bearings supporting the rotor, separately. The authors claimed that viscoelastic supports are an efficient alternative for vibration control of rotating machines.

Cavalini et al. (2011) used a smart spring mechanism (SSM) to reduce the lateral vibrations of a rotating shaft. The SSM uses an indirect piezoelectric stack actuation, imposing changes in the stiffness of one or more bearings of the rotating machine to suppress the vibration amplitudes. The proposed semi-active vibration control approach was effective for the three tested conditions, namely impact applied to the rotor during a transient operation, impact applied to the rotor operating on a constant rotating speed, and impact applied to the rotor at rest.

According to Carvalho et al. (2021), the active vibration control approaches are the most adaptable ones for rotating machines, allowing for dynamic control forces to be applied to different frequency ranges. Electromechanical shakers, PZT stacks, EMAs, and AMBs have been used as actuators for active vibration control in rotating shafts. Wickramasinghe et al. (2008) claim that the vibration suppression obtained with active techniques depends on the displacement capability of the actuators chosen, being sometimes expensive and complex to use.

In various applications, control techniques have been used in rotating machines aiming at reducing their lateral vibration amplitudes. Different researchers have shown that such reduction can improve the efficiency of the rotor, Karakaya, Karakas (2014). Nevertheless, it should be noticed that several types of control approaches are available, so that the most effective approach should be chosen for a particular application.

According to Cavalini et al. (2011), passive vibration control is obtained by modifying the dynamic characteristics of the machine, including mass, stiffness, or damping, as can be seen in Ribeiro et al. (2015). Otherwise, semi-active techniques aim at changing the physical parameters of rotating machines, as shown in Jung, DeSmidt (2018). Finally, active control strategies are based on the application of dynamic forces

to the rotating shaft to reduce its lateral vibrations, Tammi (2007). Essentially, an active vibration system is composed of sensors, actuators, and a controller, as demonstrated by Carvalho et al. (2021), where a fuzzy controller was applied to a rotor supported by active magnetic bearings.

Considering the contribution from Koroishi et al. (2014), the attenuation of lateral vibrations can prevent premature failures in the components of rotating machines, decreasing unexpected shutdowns and maintenance cost, considerably. In this context, the present contribution proposes a vibration control-based technique devoted to shafts with cracks, aiming to minimize its propagation. For this aim, a PID active control technique is applied to suppress the $2X$ and $3X$ vibration amplitudes of a cracked rotating shaft. Numerical and experimental results obtained from the proposed control law are presented and compared. In this case, the control law applies a band-pass filter to the vibration displacement responses of the rotating machine, focusing on generating control currents containing only $2X$ and $3X$ super-harmonics. Consequently, the control effort is concentrated on the frequency range for which the vibration response has to be attenuated.

Over the years, academic works have been dedicated to understanding the dynamic behavior of cracked shafts, while new vibration control techniques were proposed for improving the dynamic responses of rotating machines. Therefore, in the present work, the control effort applied to the rotor is not focused on reducing the overall lateral vibration amplitudes. Moreover, the controller was designed to reduce only the $2X$ and $3X$ super-harmonic vibration responses of the rotor, aiming to suppress the effects of the considered transverse crack affecting the shaft.

Chapter 2

Materials and Methods

2.1 Rotor Model

According to Lalanne, Ferraris (1988), the mathematical model capable of representing the dynamic behavior of a rotating machine is given by:

$$M\ddot{q} + [D + \Omega D_g]\,\dot{q} + Kq = W + F_u + F_{control} + \Delta Kq \tag{2.1}$$

where M stands for the mass matrix, D represents the damping matrix, D_g is the gyroscopic effect, and K is the stiffness matrix. These matrices are related to moving parts of the rotating machine, such as discs, couplings, and the shaft. The generalized coordinate vector is represented by q, the rotating speed is given by Ω, W stands for the weight force, F_u is the unbalance force, and $F_{control}$ represents forces determined using the vibration control approach. In this case, ΔK stands for a stiffness matrix associated with the crack.

The Timoshenko beam theory associated with the FE method were used to determine the matrices presented in Eq. (2.1), considering four degrees-of-freedom (DoF) with two displacements (u_i and w_i; $i = 1, 2$) and two rotations (θ_i and φ_i; $i = 1, 2$).

The FE model of the rotating shaft leads to high-order matrices. Due to the computational cost required for the time integration of Eq. (2.1), it is convenient to consider the system of equations described in the modal domain by taking into account only the vibration modes of interest. In the present contribution, the so-called pseudo-modal method was used to convert Eq. (2.1) from the time to the modal domain by using the first twelve natural modes of the rotating machine, Lalanne, Ferraris (1988).

2.2 Transverse crack model

The existence of a transverse crack in a rotating shaft leads to variable mechanical stiffness, according to the angular position of the crack, Kulesza, Sawicki (2012). Transverse cracks occur due to the fatigue process associated with the variable nature of the loads involved in rotating machines. Fatigue cracks present near-zero width, generating the so-called breathing mechanism in which the crack opens when facing down and closes when facing up due to the weight of a horizontal shaft Dimarogonas (1996) and Morais et al. (2020).

In the present work, the Mayes model was chosen to simulate the crack behavior. The Mayes model considers a smooth transition from the fully open to the fully closed crack, according to the angular position of the rotor. In this case, the additional flexibility introduced in the shaft due to the crack depth was determined from the linear fracture mechanics theory, Anderson (2017).

Two coordinate frames are used to model the cracked shaft, namely OXZ and $O\eta\xi$ (see Fig. 2.1). The former reference frame is fixed in space and the second one rotates according to the rotor position.

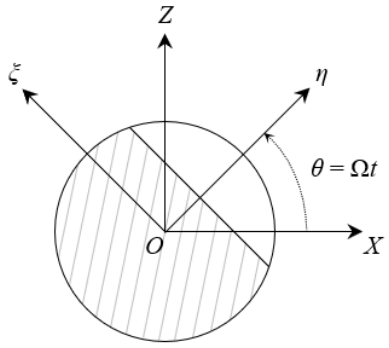

Figure 2.1: Cross-section of the cracked element, in which the hashed area represents the healthy part of the rotor and the white area indicates the crack depth (θ is the angular position of the shaft and t is the time; $\theta = \Omega t$).

The stiffness of the cracked shaft along the η and ξ directions according to the Mayes model, can be defined as:

$$k_{\eta_{Mayes}}(\theta) = \frac{1}{2}(k_o + k_\eta) + \frac{1}{2}(k_o - k_\eta)C_1$$

$$k_{\xi_{Mayes}}(\theta) = \frac{1}{2}(k_o + k_\xi) + \frac{1}{2}(k_o - k_\xi)C_1 \tag{2.2}$$

where $k_{\eta_{Mayes}}$ and $k_{\xi_{Mayes}}$ stand for the angular dependent stiffness along the η and ξ directions, respectively; k_o is the stiffness of the healthy shaft; and k_η and k_ξ are the stiffness of the shaft with a crack along the η and ξ directions, respectively ($C_1 = cos\theta$). Thus, if $\theta = 0$ degrees and the stiffness $k_{\eta_{Mayes}}(0) = k_{\xi_{Mayes}}(0) = k_o$, the crack remains fully closed. On the other hand, if $\theta = 180$ degrees, the stiffness $k_{\eta_{Mayes}}(180) = k_\eta$, and $k_{\xi_{Mayes}}(180) = k_\xi$, the crack remains fully open, Cavalini Jr et al. (2016).

The stiffness of the shaft with crack in rotating coordinates according to the Mayes model is given by:

$$\mathbf{k}_{R_{Mayes}} = \begin{bmatrix} k_{M\xi} + k_{D\xi}C_1 & 0 \\ 0 & k_{M\eta} + k_{D\eta}C_1 \end{bmatrix} \tag{2.3}$$

where $k_{M\xi} = (k_o + k_\xi)/2$, $k_{M\eta} = (k_o + k_\eta)/2$, $k_{D\xi} = (k_o - k_\xi)/2$, and $k_{D\eta} = (k_o - k_\eta)/2$.

Therefore, the stiffness of the shaft with crack in fixed coordinates is obtained as follows:

$$\mathbf{k}_{F_{Mayes}} = \begin{bmatrix} C_1 & S_1 \\ -S_1 & C_1 \end{bmatrix}^T \mathbf{k}_{R_{Mayes}} \begin{bmatrix} C_1 & S_1 \\ -S_1 & C_1 \end{bmatrix} \tag{2.4}$$

$$\mathbf{k}_{F_{Mayes}} = \begin{bmatrix} k_{FMayes11} & k_{FMayes12} \end{bmatrix}$$

where $S_1 = sin\theta$.

The stiffness terms $k_{FMayes11}$ and $k_{FMayes22}$ are included in the FE formulation to obtain the stiffness matrix K_c of the shaft element with crack. Consequently, the stiffness matrix associated with the crack presented in Eq. (2.1) can be determined as follows:

$$\Delta K = K_p - K_c \tag{2.5}$$

in which K_p is the stiffness matrix of the pristine shaft element where the crack will be included. Note that the crack is incorporated into the FE model by considering a time-dependent force. This force takes into account the variation of the mechanical stiffness of the shaft as caused by the crack and the displacements at the position of the cracked element.

2.3 Rotor test-rig

Figure 2.2a presents the test-rig used to evaluate the proposed crack control technique. It is composed by a horizontal steel shaft with 17 mm diameter and 930 mm

length (Young's modulus $E = 182GPa$, density$\rho = 7930kg/m^3$, and Poisson $\mu = 0.29$), two rigid steel discs (D_1 and D_2; 150 mm diameter and 20 mm thickness), one hybrid bearing (B_1; self-aligning ball bearing with EMAs), and one self-aligning ball bearing (B_2). A FE model with 31 elements was used to represent this system, as shown in Fig. 2.2b. The vibration responses of the rotor were measured by using four proximity probes located at the positions corresponding to the nodes $\#16$ and $\#22$ of the FE model (sensors S_{16X}, S_{16Z}, S_{22X}, and S_{22Z}).

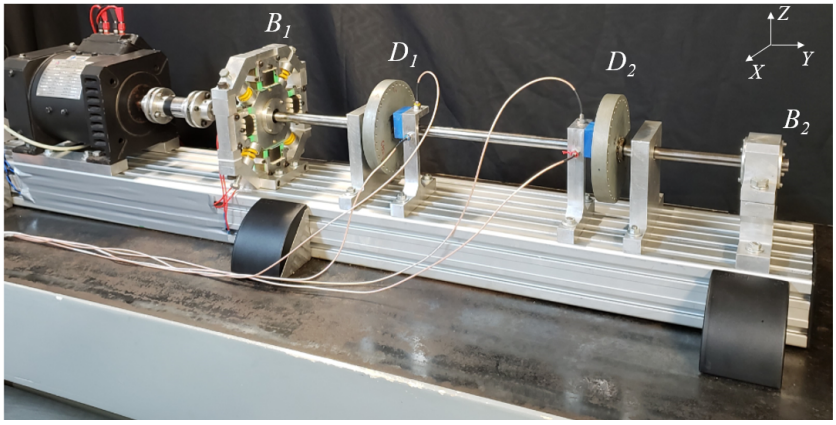

(a)

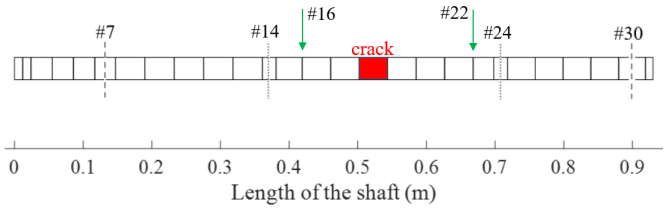

(b)

Figure 2.2: The test rig used in the present contribution is presented in (a). The FE mesh used to represent the rotating machine can be seen in (b), as well as the position of the crack.

Figure 2.2b shows the position in which the saw cut was machined along the shaft diameter (50% depth). In this case, a more realistic crack behavior was obtained by introducing a shim in the crack area intending to simulate the breathing mechanism.

Electromagnetic actuators (EMA) were used in the experimental tests to apply the control effort on the rotating machine. Figure 2.2a presents the hybrid bearing B_1 (self-aligning ball bearing with EMAs) of the rotating machine used for vibration control

purposes. In this case, the horizontal and vertical external forces can be applied to the rotating shaft through the four EMAs disposed along these two directions.

The EMAs used in the hybrid bearing are composed of an E shaped part, called *core*, and an I shaped part, called *target*. The *target* is fixed to the housing of the self-aligning ball bearing, enabling the active control forces to be applied. The distance between the E and I parts can be adjusted using a sliding apparatus. In this case, the gap e was set to be $500\ \mu m$ for all EMAs. Therefore, attraction forces up to 150 N for an electric current of 2.5 A can be obtained. Table 2.1 presents the physical and geometric properties of the EMAs. Figure 2.3 shows the schematic representation of the EMAs used in this contribution.

Table 2.1: Physical and geometric properties of the EMAs.

Variable	Value
μ_o	$4\pi 10^{-7}\ H/m$
N	250 windings
a	$9.5\ mm$
b	$38\ mm$
c	$28.5\ mm$
d	$9.5\ mm$
e	$0.5\ mm$
f	$20.5\ mm$

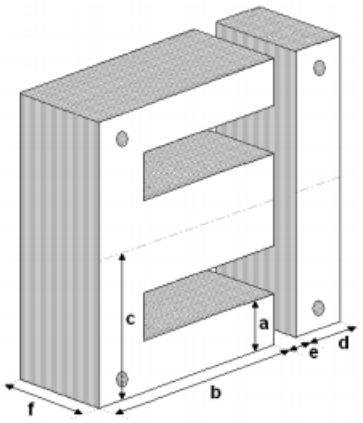

Figure 2.3: Schematic representation of the EMAs used in this contribution.

The force produced by each EMA used in the hybrid bearing can be obtained ac-

cording to Eq. (2.6).

$$F_{ema} = \frac{N^2 I^2 \mu_o a f}{2((e \pm \delta) + \frac{b+c+d-2a}{\mu_r})^2} \tag{2.6}$$

where N is the number of windings; I is the electrical current crossing the coil; a, b, c, d, e, and f are dimensions of the EMAs; μ_o is the vacuum magnetic permeability (see Table 2.1); μ_r is the relative magnetic permeability of each EMA; and δ stands for the shaft vibration, which continuously alters the distance $e \pm \delta$ between the E and I parts.

Further information about EMAs used in this work can be found in Koroishi et al. (2014).

2.4 Model updating

In the present contribution, the Differential Evolution approach was used to determine the unknown parameters of the rotating machine based on numerical and experimental frequency response functions (FRFs), Storn, Price (1997).

Nine unknown parameters of the FE model were determined, namely the stiffness along both vertical and horizontal directions of each bearing ($k_{XX_{B1}}$, $k_{ZZ_{B1}}$, $k_{XX_{B2}}$, and $k_{ZZ_{B2}}$); the modal damping factors associated with the first four vibration modes (ξ_1, ξ_2, ξ_3, and ξ_4); and the torsional stiffness $k_{t_{coup}}$ due to the coupling between the shaft and the electric motor.

Experimental FRFs were determined from the test-rig at rest for the pristine shaft, considering impacts applied separately along the horizontal and vertical directions of both discs and the vibration responses measured by the sensors S_{16X}, S_{16Z}, S_{22X}, and S_{22Z} (measurement performed along the same direction of the impact). Therefore, eight FRFs were obtained from 0 to $100\ Hz$ with steps of $0.25\ Hz$.

In this case, the optimization process was performed 10 times considering 90 individuals used in the initial population of the optimizer (10 individuals for each parameter to be optimized), $F_{DE} = 0.8$, and $CR_{DE} = 0.5$. Equation (2.7) shows the objective function F_{DE} used in the minimization process.

$$F_{DE} = \sum_{k=1}^{n} \frac{||FRF_{exp,\,k} - FRF_{num,\,k}||}{||FRF_{exp,\,k}||} \tag{2.7}$$

where $FRF_{exp,k}$ stands for the experimental FRFs, $FRF_{num,k}$ represents the numerical

FRFs, and $n = 8$ (number of FRFs). It is worth mentioning that only the regions close to the peaks associated with the vibration modes were considered to determine F_{DE}.

Figure 2.4 presents one of the numerical FRFs obtained by using the updated FE model with the optimum parameters shown in Table 2.2. The corresponding experimental curve is also presented for comparison purposes (similar results were obtained with the other FRFs). Note that the updated FE model is able to represent satisfactorily the dynamic behavior of the rotating machine in the adopted frequency range. Two natural frequencies associated with the vertical direction of the rotor at rest are shown in Fig. 2.4. Two natural frequencies are also observed along with the horizontal direction of the rotor. These four natural frequencies lead to four critical speeds when the rotor is under operation.

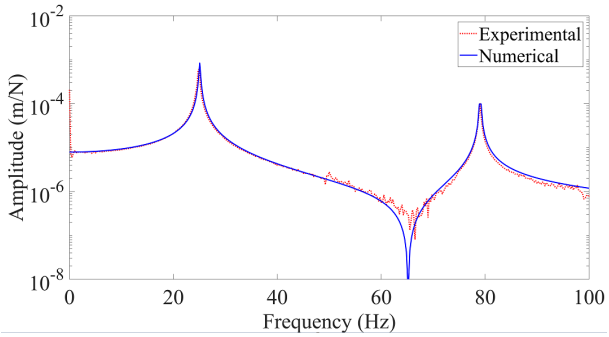

Figure 2.4: Numerical FRF determined using the updated FE model and the corresponding experimental curve: excitation along the vertical direction of D_1 and vibration measurement performed using the sensor S_{16Z}.

Therefore, the first four critical speeds of the rotor were found to be $1,474\ rev/min$ ($24.56\ Hz$), $1,506\ rev/min$ ($25.10\ Hz$), $4,482\ rev/min$ ($74.70\ Hz$), and $4,753\ rev/min$ ($79.22\ Hz$).

2.5 Controller design

The strategy used to apply the control efforts to the shaft is presented in Fig. 2.5. In this case, the EMA$\#1$ and EMA$\#3$ are used to apply the vertical forces (Z direction), while the horizontal forces are applied through the EMA$\#2$ and EMA$\#4$. Figure 2.5b shows the currents applied to each EMA so that the shaft reproduces a circular orbit. Additionally, a bias current of 50 mA was considered for keeping the EMAs core

Table 2.2: Results obtained in the FE model updating process and the limits considered for each unknown parameter in the optimization (k $[N/m]$ and $k_{t_{coup}}$ $[Nm/rad]$).

Parameter	Lower limit	Optimum	Upper limit
$k_{XX_{B1}}$	5×10^5	8.55×10^5	5×10^6
$k_{ZZ_{B1}}$	5×10^5	5.21×10^7	1×10^7
$k_{XX_{B2}}$	5×10^7	1.19×10^6	1×10^9
$k_{ZZ_{B2}}$	5×10^7	7.02×10^8	1×10^9
ξ_1	1×10^{-5}	9.02×10^{-3}	1×10^{-2}
ξ_2	1×10^{-5}	9.92×10^{-2}	1×10^{-2}
ξ_3	1×10^{-5}	9.01×10^{-3}	1×10^{-2}
ξ_4	1×10^{-5}	3.01×10^{-2}	1×10^{-2}
$k_{t_{coup}}$	0	5.54×10^2	1×10^3

energized, providing a faster actuation. This value was found to be small enough to not increase the EMAs temperatures and high enough to keep them energized during operation.

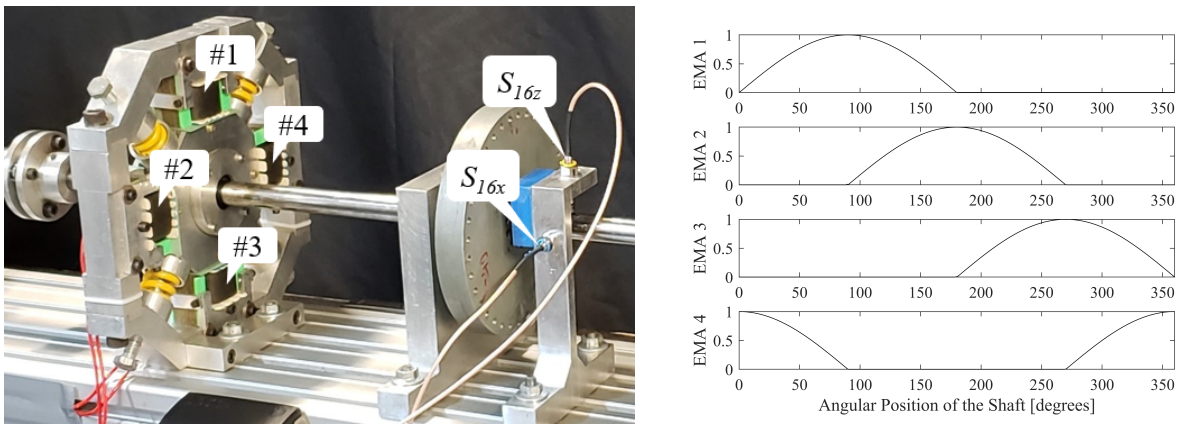

(a) (b)

Figure 2.5: (a) Distribution of the EMAs in the hybrid bearing presenting two actuators for each direction and (b) the currents applied to each EMA to the shaft reproduce a circular orbit.

In the present work, a closed-loop control approach was formulated by adding a controller before the open-loop plant, as shown in Fig. 2.6.

According to Visioli (2006), the PID control is the most commonly used approach in

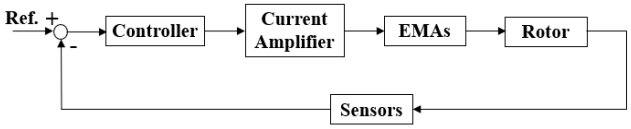

Figure 2.6: Closed-loop plant representing the control setup used in the present contribution.

the industry due to its efficiency and simplicity. Therefore, this technique was adopted in the present contribution. Equation (2.8) presents the parallel continuous PID control expression.

$$PID = \frac{K_D s^2 + K_P s + K_I}{s} \tag{2.8}$$

where K_D represents the derivative gain, K_P is the proportional gain, and K_I is the integral gain.

The rotor of the present work has an inverse K_P relationship since the direction of the control forces is opposite to the direction of the shaft displacement. Additionally, experimental tests reveal a faster control actuation when K_D was used. However, K_I was observed not influencing the system due to the springs of the hybrid bearing that support the shaft at the bearing center. The rotor does not present steady-state error to be compensated for and, consequently, a PD controller can be used in the present contribution.

The inputs of the PD controller are the lateral vibrations of the shaft measured by using the sensors S_{16X} and S_{16Z} (see Fig. 2.5a). The outputs of the controller are the electric currents applied to the EMAs. Therefore, probe S_{16X} was considered to be the reference to generate the control currents applied to EMA$\#2$ and EMA$\#4$, while S_{16Z} was the reference adopted for the control currents applied to the EMA$\#1$ and EMA$\#3$. The logic of the controller is presented in Fig. 2.6.

In the present contribution, a PD control with a first order butterworth bandpass filter was applied in the frequency range corresponding to the $2X$ and $3X$ super-harmonic vibration components (crack signatures). This approach generates control currents containing frequencies in a range between the $2X$ and $3X$ super-harmonic vibration responses of the shaft. Such configuration may reduce the influence of the crack on the dynamic behavior of the rotor, decelerating its propagation. Therefore, the proposed methodology was evaluated by considering three different rotation speeds, namely:

1. $\Omega = \Omega_{crit}/3 = 491.3\ rev/min$;
2. $\Omega = \Omega_{crit}/2 = 737\ rev/min$;
3. $\Omega = \Omega_{operation} = 900\ rev/min$.

where Ω_{crit} is the backward first critical speed of the rotating machine.

It is worth mentioning that high vibration amplitudes were achieved with the rotating machine operating at $\Omega = \Omega_{crit}/3 = 491.3\ rev/min$ and $\Omega = \Omega_{crit}/2 = 737\ rev/min$. Therefore, the experimental tests were performed with the rotor operating at $489\ rev/min$ and $705\ rev/min$, respectively.

Chapter 3

Numerical and experimental results

The numerical and experimental results obtained using the PD active controller are presented in this section. In all test cases, an unbalance of $4.26 \times 10^{-4}\ Kgm/-90^{o}$ was applied to the disc D_1. Additionally, the vibration responses were measured considering the rotor operating in a steady-state condition. Therefore, the effectiveness of the evaluated PD control strategy is demonstrated through vibration responses in the frequency domain and shaft orbits. It is worth mentioning that all tests were performed for the shaft with crack (see Fig. 2.2).

3.1 Rotation speed: $\Omega \simeq \Omega_{\mathbf{crit}}/3 \simeq 489\ \mathbf{rev/min}$

The PD gains adopted for $\Omega \simeq \Omega_{crit}/3 \simeq 489\ rev/min$ considering the application with filter were: $K_P = -100$ and $K_P = 8$ in the numerical tests; and $K_P = -180$ and $K_P = 1$ in the experimental tests. Figures 3.1a and 3.1b show the numerical frequency vibration responses obtained using the PD control strategy of this section. The corresponding experimental results are presented in Figs. 3.1d and 3.1e. Note that the $3X$ super-harmonic vibration amplitude was reduced with the control action in both numerical (32.7% - horizontal direction; 0.6% - vertical direction) and experimental tests (46.7% - horizontal direction; 95.5% - vertical direction). The dynamic behavior of the shaft before and after the control action can be observed in the numerical and experimental orbits of the Fig. 3.1c and Fig. 3.1f, respectively. Note that the vibration reduction is more evident in the experimental test. However, vibration attenuation can be observed in the numerical results. Similar results were obtained using the sensors

S_{22X} and S_{22Z}.

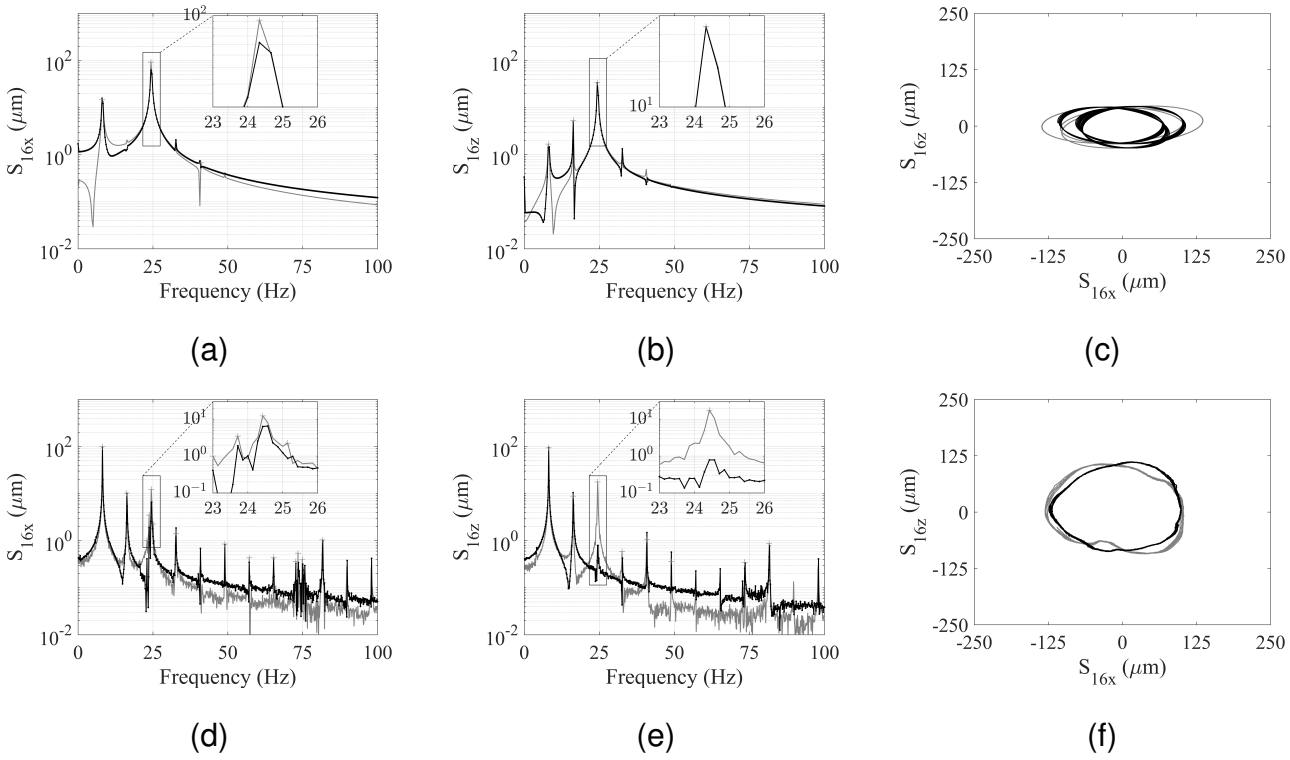

Figure 3.1: Results obtained for $\Omega = 489\ rev/min$ and using the PD controller with filter (— control OFF; — control ON). Numerical results: (a) sensor S_{16X}, (b) sensor S_{16Z}, and (c) orbit. Experimental results: (c) sensor S_{16X}, (d) sensor S_{16Z}, and (e) orbit.

Concerning the frequency response of the simulated rotor, a subtle decrease can be noticed on the $3X$ super-harmonics on both vertical and horizontal directions (see Figs. 3.1a and 3.1b). On the other hand, an increase on the vibration amplitudes of the $2X$ super-harmonic can be observed in the horizontal direction. Figure 3.1e shows that the $3X$ super-harmonic vibration amplitude decrease significantly with the control action in the experimental tests.

3.2 Rotation speed: $\Omega \simeq \Omega_{\mathbf{crit}}/2 \simeq 705\ \mathbf{rev/min}$

The PD gains adopted for $\Omega \simeq \Omega_{crit}/2 \simeq 705\ rev/min$ considering the application with filter were: $K_P = -200$ and $K_P = 40$ in the numerical tests; and $K_P = -200$ and $K_P = 1.5$ in the experimental tests. Figures 3.2a and 3.2b show the numerical frequency vibration responses obtained using the PD control strategy of this section.

The corresponding experimental results are presented in Figs. 3.2d and 3.2e. Note that the $2X$ super-harmonic vibration amplitude was reduced with the control action in both numerical (30.4% - horizontal direction; 21.3% - vertical direction) and experimental tests (43.4% - horizontal direction; 50.7% - vertical direction). The dynamic behavior of the shaft before and after the control action can be observed in the numerical and experimental orbits of the Fig. 3.2c and Fig. 3.2f, respectively. Note that vibration reduction is obtained in both numerical and experimental tests. Similar results were obtained using the sensors S_{22X} and S_{22Z}.

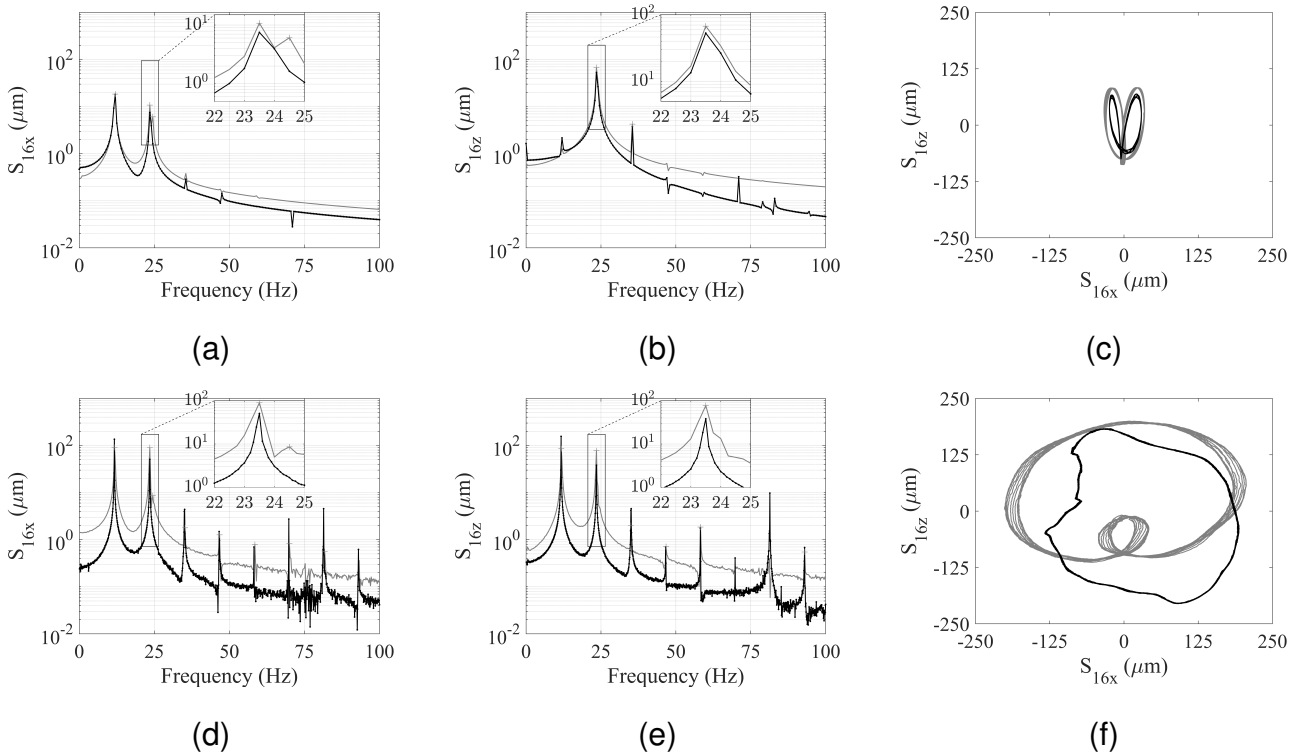

Figure 3.2: Results obtained for $\Omega = 705\ rev/min$ and using the PD controller with filter (— control OFF; — control ON). Numerical results: (a) sensor S_{16X}, (b) sensor S_{16Z}, and (c) orbit. Experimental results: (c) sensor S_{16X}, (d) sensor S_{16Z}, and (e) orbit.

Figures 3.2d and 3.2e show that the $1X$ and $3X$ super-harmonic vibration amplitudes (and some higher components) increase with the control action in the experimental tests, which is considered as being a side effect since such an increase on these vibration components is small as compared with the attenuation obtained at the $2X$ frequency response.

As mentioned, the purpose of the proposed active control approach is to decrease especially the $2X$ and $3X$ super-harmonic vibration amplitudes of the rotor to attenuate

the effects of a transverse crack on the horizontal shaft. Therefore, Fig. 3.2e shows that the inner loop of the orbits measured in the rotor test-rig was attenuated with the control action. Consequently, it can be concluded that the corresponding effects of the crack on the shaft were also attenuated in the present context.

3.3 Rotation speed: $\Omega = 900$ rev/min

The PD gains adopted for $\Omega = \Omega_{operation} = 900\ rev/min$ considering the application with filter were: $K_P = -1000$ and $K_P = 90$ in the numerical tests; and $K_P = -400$ and $K_P = 10.4$ in the experimental tests. Figures 3.3a and 3.3b show the numerical frequency vibration responses obtained using the PD control strategy of this section. The corresponding experimental results are presented in Figs. 3.3d and 3.3e. The numerical and experimental orbits are presented in Figs. 3.3c and 3.3f, respectively. Note that the vibration amplitudes of the rotor were not reduced efficiently with the control action in both numerical ($2X$ component; 0.2% - horizontal direction; 0.1% - vertical direction) and experimental tests ($2X$ component; 26.5% - horizontal direction; 18.4% - vertical direction).

Note that no significant variation on the vibration responses of the representative FE model is observed with the controller action with the rotor operating at 900 rev/min. However, vibration attenuation was achieved in the experimental tests. This speed is an asynchronous rotation speed, therefore the corresponding super-harmonic amplitudes are expected to be low, impairing the action of the controller.

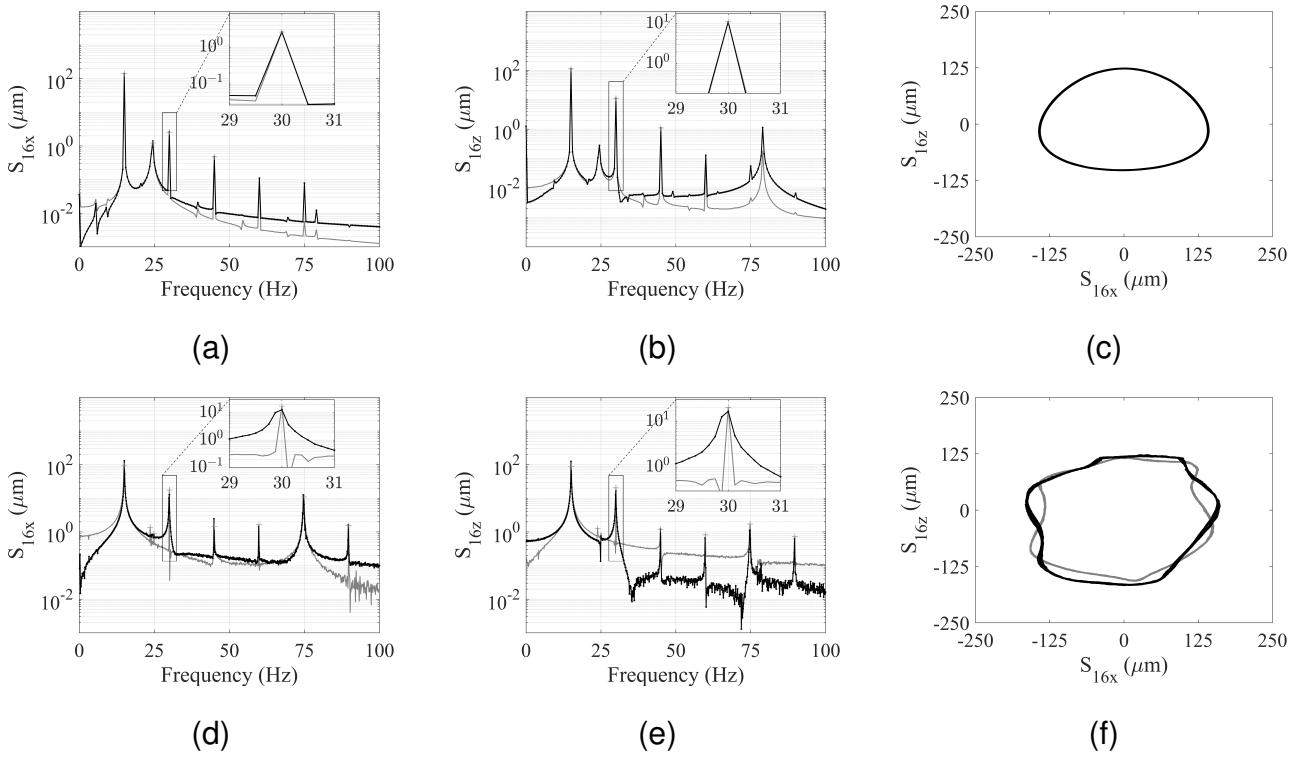

Figure 3.3: Results obtained for $\Omega = 900\ rev/min$ and using the PD controller with filter (— control OFF; — control ON). Numerical results: (a) sensor S_{16X}, (b) sensor S_{16Z}, and (c) orbit. Experimental results: (c) sensor S_{16X}, (d) sensor S_{16Z}, and (e) orbit.

3.4 Summary of Results

The results associated with the proposed crack active control are summarized in this section. Table 3.1 presents the reduction on the vibration amplitudes obtained using the proposed control law, namely PD control with filter on the range between the $2X$ and $3X$ super-harmonics. The vibration reduction obtained by using the control currents being generated based on the overall displacement of the rotor (PD control without filter) are shown in Table 3.2 for comparison purposes. Note that the proposed control approach was effective in most test cases. Additionally, when compared with the tests performed using the PD control without filter, better results were obtained by the proposed approach for the corresponding experimental tests performed with the rotor operating at 900 rev/min.

Table 3.1: Results obtained using the PD control with filter.

Rotation	Horizontal direction; reduction (%)		
speed (rev/min)	Harmonic	Numerical	Experimental
489	$3X$	32.7	46.7
705	$2X$	30.4	43.4
900	$2X$	0.2	26.5

Rotation	Vertical direction; reduction (%)		
speed (rev/min)	Harmonic	Numerical	Experimental
489	$3X$	0.6	95.5
705	$2X$	21.3	50.7
900	$2X$	0.1	18.4

Table 3.2: Results obtained using the PD control without filter.

Rotation	Horizontal direction; reduction (%)		
speed (rev/min)	Harmonic	Numerical	Experimental
489	$3X$	84.9	70.6
705	$2X$	32	62.4
900	$2X$	7.3	0.3

Rotation	Vertical direction; reduction (%)		
speed (rev/min)	Harmonic	Numerical	Experimental
489	$3X$	58.7	93.3
705	$2X$	24.1	53.3
900	$2X$	0.2	0.4

Chapter 4

Conclusions

The present work aimed at improving rotating machinery lifetime, reliability, and reducing scheduled maintenance frequency by decreasing the transverse crack effects on rotating shafts. For this purpose, a crack control approach was proposed in the present contribution. Numerical and experimental tests were performed to evaluate the effectiveness of the conveyed approach. A PD controller was designed based on two different control laws aiming at suppressing the signatures of a transverse crack, namely a PD control without filtering the vibration responses of the rotor, and a PD control using a first order butterworth bandpass filter applied in the frequency range corresponding to the $2X$ and $3X$ super-harmonic components of the rotor vibration responses (crack signatures). It is worth mentioning that both control laws were tested in the following rotation speeds: $491.3\ rev/min$ ($\Omega \simeq \Omega_{crit}/3$), $737\ rev/min$ ($\Omega \simeq \Omega_{crit}/2$), and $900\ rev/min$. The difference between the gains obtained in the numerical and experimental tests can be associated with the lack of representativeness of the adopted model. In this case, the dynamic behavior of the EMAs is described as given by Eq. (2.6). However, current losses and geometrical imperfections present on the actuators installed in the rotor are not considered in their mathematical model. The results demonstrated that the first control law was more efficient for suppressing the crack signatures for the $\Omega_{crit}/2$ and the $\Omega_{crit}/3$. However, this control approach was not able to suppress the crack signatures (the $2X$ and $3X$ super-harmonics) for the asynchronous rotation speed of $900\ rev/min$. On the other hand, the addition of a bandpass filter to the active controller allowed to decrease the effect of a transverse crack on the experimental tests. The proposed control law was also able to suppress the crack signatures

with the rotor operating at $\Omega_{crit}/2$ and $\Omega_{crit}/3$, however with a smaller efficiency as compared with the first control approach. Therefore, the results indicated the effectiveness of the proposed crack control approaches for rotating machines regarding real-world applications. Further research effort will be dedicated to perform more experimental tests considering different faults affecting the rotor, as well as other operating conditions and filters applied to the rotor vibration responses.

References

Anderson T L. Fracture mechanics: fundamentals and applications. 3rd ed. 10 2017. 688.

Bachschmid N., Pennacchi Paolo, Tanzi E., Vania A. Identification of Transverse Crack Position and Depth in Rotor Systems // Meccanica. 11 2000. 35. 563–582.

Boyko Alexander, Popov Sergey, Krajisnik Nemanja. Investigating the Sayano-Shushenskaya Hydro Power Plant Disaster // Power. 12 2010. 154.

Camino J. F., Santos I. F. A periodic linear–quadratic controller for suppressing rotor-blade vibration // Journal of Vibration and Control. 2019. 25, 17. 2351–2364.

Carden E. Peter, Fanning Paul. Vibration Based Condition Monitoring: A Review // Structural Health Monitoring. 2004. 3, 4. 355–377.

Carvalho Felipe Carmo, Oliveira Marcus V Fernandes de, Lara-Molina Fabian A, Aldemir A Cavalini Jr, Valder Steffen Jr. Fuzzy robust control applied to rotor supported by active magnetic bearing // Journal of Vibration and Control. 2021. 27, 7-8. 912–923.

Cavalini Aldemir Ap., Morais Thiago Vianna Galavottiand Tobias Souza, Koroishi Edson Hideki, Steffen Valder. Vibration attenuation in rotating machines using smart spring mechanism // Mathematical Problems in Engineering. 2011. 2011, 340235. 1–14.

Cavalini Jr A.A., Sanches L., Bachschmid N., Steffen Jr V. Crack identification for rotating machines based on a nonlinear approach // Mechanical Systems and Signal Processing. 2016. 79. 72–85. Special Issue from ICEDyn 2015.

CavaliniJr Aldemir A, Morais Tobias S, Silva Izabela B da, Bachschmid Nicolò, SteffenJr Valder. Investigation of the favorable conditions to apply the combination resonances approach for crack detection purposes // Journal of Vibration and Control. 2020. 26, 15-16. 1345–1355.

Demierre J., Henchoz S., Favrat D. Prototype of a thermally driven heat pump based on integrated Organic Rankine Cycles (ORC) // Energy. 2012. 41, 1. 10–17. 23rd International Conference on Efficiency, Cost, Optimization, Simulation and Environmental Impact of Energy Systems, ECOS 2010.

Demierre Jonathan, Rubino Antonio, Schiffmann Jürg. Modeling and Experimental Investigation of an Oil-Free Microcompressor-Turbine Unit for an Organic Rankine Cycle Driven Heat Pump // Journal of Engineering for Gas Turbines and Power. 10 2014. 137, 3. 032602.

Dimarogonas Andrew, Paipetis Stefanos, Chondros T.G. Analytical methods in rotor dynamics. 2nd ed. 9. 01 2013.

Dimarogonas Andrew D. Vibration of cracked structures: A state of the art review // Engineering Fracture Mechanics. 1996. 55, 5. 831–857.

Fitzgerald Breiffni, Sarkar Saptarshi, Staino Andrea. Improved reliability of wind turbine towers with active tuned mass dampers (ATMDs) // Journal of Sound and Vibration. 2018. 419. 103–122.

Friswell M I, Litak G, Sawicki J T. Crack identification in rotating machines with active bearings // Proceedings of the 24th International Conference on Noise and Vibration Engineering (ISMA 2010). 2010. 1. 1–10.

Grabowski B. The Vibrational Behaviour of a Rotating Shaft Containing a Transverse Crack // Dynamics of Rotors: Stability and System Identification. Vienna: Springer Vienna, 1984. 5, 423–465.

Greco J, Agnew J R, Erhardt K, Bertilsson J E, Stys Z S. Cumberland Steam Plant: cracked IP rotor coupling of Unit 2 // Proc. Am. Power Conf.; (United States). 1 1978. 40.

Jeon Ikgeun, Lim Hyung Jin, Liu Peipei, Park Byeongjin, Heinze Andreas, Sohn Hoon. Fatigue crack detection in rotating steel shafts using noncontact ultrasonic modulation measurements // Engineering Structures. 2019. 196. 109293.

Jung DaeYi, DeSmidt Hans. A new hybrid observer based rotor imbalance vibration control via passive autobalancer and active bearing actuation // Journal of Sound and Vibration. 2018. 415. 1–24.

Karakaya Abdulhakim, Karakas Ercument. Implementation of neural network based maximum power tracking control for wind turbine generator // Turkish Journal of Electrical Engineering and Computer Sciences. 11 2014. 22. 1410–1422.

Klompas N. Effects of Anomalous Rotor Joints on Turbomachine Dynamics // Proceedings of the ASME Turbo Expo: Power for Land, Sea, and Air. 1983. 5. V005T12A017.

Koroishi Edson Hideki, Borges Adriano Silva, Cavalini Aldemir Ap, Steffen Valder. umerical and experimental modal control of flexible rotor using electromagnetic actuator // Mathematical Problems in Engineering. 2014. 2014, 361418. 1–14.

Kottke J K, Menning R H. Detection of a transverse crack in a turbine shaft—the oak creek experience // Proceedings of the ASME Conference Paper 81-JPGC-Pwr-19. 1981. 1. 303–307.

Kulesza Zbigniew, Sawicki Jerzy T. Rigid finite element model of a cracked rotor // Journal of Sound and Vibration. 2012. 331, 18. 4145–4169.

Lalanne Michel, Ferraris Guy. Rotordynamics prediction in engineering. 2nd ed. 2 1988. 272.

Leão L.S., Cavalini A.A., Morais T.S., Melo G.P., Steffen V. Fault detection in rotating machinery by using the modal state observer approach // Journal of Sound and Vibration. 2019. 458. 123–142.

Logan Jr Earl. Turbomachinery: basic theory and applications. 2nd ed. 6 1993. 280.

Morais Tobias Souza, Souza Leão Leandro de, Jr Aldemir Ap Cavalini, Jr Valder Steffen. Rotating machinery health evaluation by modal force identification // Inverse Problems in Science and Engineering. 2020. 28, 5. 695–715.

Nicoletti Rodrigo, Cavalini Aldemir A., Steffen Valder. Detection of Cracks in Rotating Shafts by Using the Combination Resonances Approach and the Approximated Entropy Algorithm // Shock and Vibration. 2018. 2018, 4094631. 1–14.

Ostachowicz Wiesław, Krawczuk Marek. On Modelling of Structural Stiffness Loss Due to Damage // Key Engineering Materials - KEY ENG MAT. 04 2001. 204-205. 185–200.

Pesch Alexander H., Hanawalt Stephen P., Sawicki Jerzy T. A Case Study in Control Methods for Active Magnetic Bearings // Proceedings of the Dynamic Systems and Control Conference. 2014. 1. V001T12A003.

Ribeiro Eduardo Afonso, Pereira Jucélio Tomás, Alberto Bavastri Carlos. Passive vibration control in rotor dynamics: Optimization of composed support using viscoelastic materials // Journal of Sound and Vibration. 2015. 351. 43–56.

Storn Rainer, Price Kenneth. Differential evolution: a simple and efficient adaptative scheme for global optimization over continuous spaces // Journal of Global Optimization. 1997. 11. 341–359.

Tammi Kari. Active control of radial rotor vibrations: identification, feedback, feedforward, and repetitive control methods. Aalto University, 5 2007.

Visioli Antonio. Practical PID control. 1st ed. 2006. 314.

Wickramasinghe Viresh, Chen Yong, Zimcik David. Experimental Evaluation of the Smart Spring Impedance Control Approach for Adaptive Vibration Suppression // Journal of Intelligent Material Systems and Structures. 2008. 19, 2. 171–179.